A Theoretical Study of the Potential Energy Surface and Rate Constant for an O(^{3}P) + HO$_2$ Reaction

Osamu Setokuchi,* Masaru Sato, and Sadao Matuzawa

National Institute for Resources and Environment, Onogawa 16-3, Tsukuba 305-8569, Japan

Received: October 6, 1999; In Final Form: February 2, 2000

The potential energy surface for the reaction O(^{3}P) + HO$_2$ → HO$_3$ → HO + O$_2$ and the kinetic rate constant were investigated using ab initio calculations with the multireference Møller–Plesset second-order perturbation (MRMP2) method and dynamics calculations based on the microcanonical variational theory. The MRMP2 potential energy surface is compared with those of MP2, QCISD, and B3LYP based on a single reference wave function to characterize the HO$_3$ molecule, which has a planar geometry. The MRMP2 level of theory predicts that the trans geometry will be more stable than the cis geometry, while the MP2, QCISD, and B3LYP levels of theory predict that the cis geometry will be more stable. This disagreement is due to the differences in the estimations of the central O–O bond strength at various levels of theory. The temperature dependence of the microcanonical variational rate constant, which was determined from the barrierless attractive potential energy surface in the entrance channel, is shown to agree with the data recommended by NASA. The potential energy surface, corrected for basis set superposition errors, is also used to estimate the lower limit of the rate constant at this level of theory. The contribution of direct hydrogen atom abstraction reaction to the rate constant is small at low temperature. However, the reaction is preferred over the reaction channel via HO$_3$ at the high temperatures, especially above 1000 K.

Introduction

The reaction O(^{3}P) + HO$_2$ → HO + O$_2$, together with O + HO → H + O$_2$ and OH + HO$_2$ → H$_2$O + O$_2$, is an elementary reaction process that governs HO$_x$ radical concentration in the upper stratosphere[1] and mesosphere[2,3] and plays an important role in ozone atmospheric chemical reactions. Many experimental kinetic studies have been conducted to determine the rate constant for this reaction.[4–8] The reaction rate constant recommended by the NASA kinetics data evaluation panel[9] is the average of these five studies at room temperature, fitted to the temperature dependence given by two studies.[4,8] Recent modeling studies[2,3] have shown that the atmospheric chemistry reaction model that uses the recommended value for this reaction rate underestimates the ozone concentration in the mesosphere (known as the ozone deficit problem). A reevaluation of the experimental rate constant has thus been proposed.

An ^{18}O isotope labeling experiment[10] demonstrated that the reaction proceeds via abstraction of the terminal oxygen atom from HO$_2$ by the O reactant. Some theoretical studies[11,12] also have indicated that the reaction proceeds via an HO$_3$ intermediate compound, and that the HO$_3$ molecule is slightly more stable than the HO + O$_2$ products,[13–16] though some theoretical studies identify HO$_3$ as a meta-stable species placed above the HO + O$_2$ dissociation limit. A recent experimental study used Fourier transform ion cyclotron resonance mass spectrometry (FTICR-MS)[17] to demonstrate that the HO$_3$ molecule is a relatively stable intermediate, i.e., 10 ± 5 kcal/mol below the HO + O$_2$ dissociation limit; the author reported that a more precise description of the theoretical potential energy surface (PES) is necessary.[18]

In this article, we report a PES that corresponds to an approximate minimum energy reaction pathway for the reaction O(^{3}P) + HO$_2$ → HO$_3$ → HO + O$_2$, produced by ab initio calculation with the multireference Møller–Plesset second-order perturbation theory (MRMP2).[19–22] The HO$_3$ molecule was characterized by comparing the MRMP2 PES with those for theories based on a single reference wave function to investigate the influence of a nondynamic electron correlation. Furthermore, we performed a dynamics calculation using the PES and compared the calculated temperature dependence of the kinetic rate constant with the experimental data. We are aware of only two theoretical studies, i.e., quasiclassical trajectory (QCT)[23] and adiabatic approach[24] calculations, on the dynamics for this reaction, where the dynamics calculations have been performed on a single-valued double many-body expansion(DMBE) potential energy surface based on UCISD ab initio calculations.[25] We will also compare our kinetic results with their results.

Method of Calculation

The cc-pVTZ, TZV(2df,2p), and TVZ(2df,2p)++ basis sets were used in the CASSCF and MRMP2 calculations, where the cc-pVTZ basis set is a Dunning's correlation-consistent basis set[26] and the TZV(2df,2p) basis set is a [5s3p] contracted triple-ζ valence basis set[27,28] with polarization orbital exponents α_d = 2.56, 0.64 and α_f = 1.4 for the oxygen atom and α_p = 2.0, 0.5 for the hydrogen atom. The TZV(2df,2p)++ basis set includes diffuse functions with the orbital exponent α_{sp} = 0.0845 for the oxygen atom and α_s = 0.036 for the hydrogen atom. These basis sets use six Cartesian d-functions and 10 f-functions. The numbering of the atoms for the title reaction system is denoted as O$_a$–O$_b$–O$_c$–H, where O$_a$ and O$_b$–O$_c$–H represent the two reacting species, i.e., the oxygen atom and hydroperoxy radicals.

We compared two complete active space self-consistent-field (CASSCF) wave functions, CAS(19,13) and CAS(7,7), to investigate the influence of the active space on the PES. All 19

---

* Corresponding author.

PE Surface and Rate Constant for an O(^{3}P) + HO$_2$ Reaction

J. Phys. Chem. A, Vol. 104, No. 14, 2000 **3205**

valence electrons in CAS(19,13) were distributed among 13 valence orbitals. However, in CAS(7,7), which is the same as in a previous work,[12] six σ-orbital electrons and a single occupied electron on a terminal oxygen atom are distributed among the occupied orbitals and the corresponding antibonding orbitals. The geometries were optimized at the CASSCF level with the cc-pVTZ or TZV(2df,2p) basis set for all degrees of freedom except a fixed $R(O_a-O_b)$ distance for the PES in the entrance channel (O + HO$_2$ → HO$_3$), and a fixed $R(O_b-O_c)$ distance for the PES in the exit channel (HO$_3$ → HO + O$_2$). MRMP2 single-point energy calculations were carried out for these optimized geometries. The geometries and energies for the HO$_3$ molecule at the MRMP2 level were compared with those at the levels of theory based on a single reference wave function (MP2, QCISD, and B3LYP), whereas in the latter, the full optimizations of the HO$_3$ intermediates were carried out at the frozen core (FC) levels with the cc-pVTZ basis sets.

We used the counterpoise method of Boys and Bernardi[29] to investigate the influence of the basis set superposition error (BSSE) on the interaction energy at the entrance channel. MRMP2 single-point energy calculations with the TZV(2df,-2p)++ basis set were performed for the geometries optimized at the CAS(19,13)/TZV(2df,2p) level, and frequencies obtained at the CAS(19,13)/TZV(2df,2p) level were used with the resulting MRMP2/TZV(2df,2p)++ PES. These data were used to calculate the rate constant based on microcanonical variational theory (μVT).[30,31] The rate constant may be written as $k(T) = Q_{el}^{GT}(T)I_{vr}(T)/\hbar\Phi^R(T)$, where $Q_{el}^{GT}(T)$ is the electronic partition function for the generalized transition state (GTS) dividing surface, $\Phi^R(T)$ is the reactants partition function per unit volume, $I_{vr}(T)=\int_0^\infty \exp(-E/kT) N_{vr}(E) \, dE$, and $\hbar$ is Planck's constant. $N_{vr}(E)$ was obtained by minimizing the GTS vibrational–rotational sum-of-states $N_{vr}^{GT}(E,s)$ with respect to the reaction coordinate s at each E. The electronic degeneracy factors for O(^{3}P) and HO$_2$ are given by $5 + 3 \exp(-227.6/T) + \exp(-325.9/T)$ and 1.

The direct hydrogen atom abstraction reaction (O–HO$_2$ reaction) was investigated using multi-configurational quasi-degenerate second-order perturbation theory (MC-QDPT2).[21] It should be noted that the MC-QDPT2 is a multi-state perturbation theory, whereas the MRMP2 is a single-state perturbation theory.

The electronic structure calculations at the CASSCF, MRMP2, and MC-QDPT2 levels were performed using the GAMESS programs.[32] The MP2, QCISD, and B3LYP calculations used GAUSSIAN94 programs.[33] The calculations of the reaction rate constant using μVT were performed by means of POLYRATE 7.9.1 code.[34]

Results and Discussion

A. PES of the Reaction via HO$_3$. The CASSCF and MRMP2 PESs based on the CAS(7,7) wave function are shown in Figure 1, and those based on the CAS(19,13) wave function are shown in Figure 2. The terminal oxygen atom of the HO$_2$ molecule has a singly occupied molecular orbital perpendicular to the molecular plane in the electronic $^2A''$ ground state. Thus, a reactant O atom approaches nearly perpendicular to the HO$_2$ molecular plane to interact with the orbital. The PES is attractive until the HO$_3$ molecule is formed. However, we can observe a difference in the shape of the PES and the geometry around the HO$_3$ critical structure, depending on the CASSCF wave function, i.e., the size of the active space. The PES at the CAS-(7,7) level has a well corresponding to the HO$_3$ molecule, whose stable geometry is nonplanar (τ(OOOH) = 93.7°). This PES is essentially the same as that obtained by Dupuis et al.[12] The
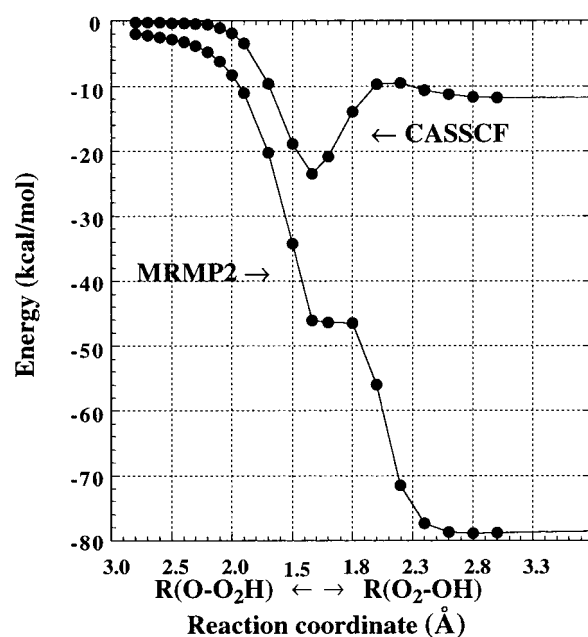

Figure 1. Potential energy surface at the MRMP2/CAS(7,7)/cc-pVTZ level.
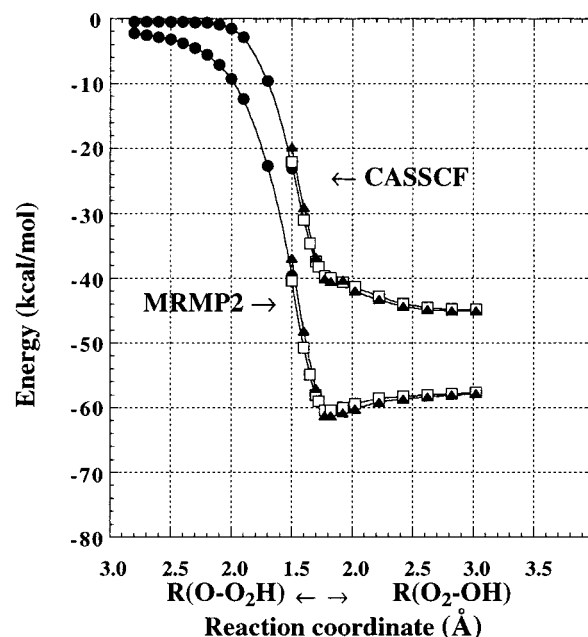

Figure 2. Potential energy surface at the MRMP2/CAS(19,13)/cc-pVTZ level: C_1-symmetry (filled circles), C_s-symmetry *cis*-HOOO (open squares), C_s-symmetry *trans*-HOOO (filled triangles).

geometry changes from nonplanar to planar at the CAS(19,13) level, as the O–O$_2$H separation becomes smaller than about 1.5 Å. Also, the HO$_3$ molecule is meta-stable relative to the products. The planarity of the HO$_3$ molecule results from the delocalization of lone pairs of electrons on the oxygen atoms. The CAS(7,7) wave function does not include lone pairs of electrons and their orbitals on the oxygen atoms in the active space, except for a singly occupied orbital on the terminal oxygen atom. As a result, the calculation does not consider such a stabilization effect due to the delocalization of lone pairs of electrons and suggests that the nonplanar geometry is a stable HO$_3$ molecule. An interesting additional feature appears when the dynamic electron correlation is taken into account for these two CASSCF wave functions. The MRMP2/CAS(7,7) calculation, with an insufficient reference wave function, describes the

TABLE 1: Energies (a.u.) for HO$_3$ Geometries^a Optimized at the Various Levels of Theory^b

	MP2		QCISD		B3LYP		CASSCF	
	cis−HO$_3$	*trans*−HO$_3$	*cis*−HO$_3$	*trans*−HO$_3$	*cis*−HO$_3$	*trans*−HO$_3$	*cis*−HO$_3$	*trans*−HO$_3$
$R(O_a-O_b)$	1.243	1.241	1.268	1.257	1.251	1.234	1.229	1.223
$R(O_b-O_c)$	1.433	1.437	1.461	1.475	1.503	1.544	1.75	1.75
$R(O_c-H)$	0.975	0.969	0.970	0.966	0.973	0.970	0.976	0.975
$\theta(O_aO_bO_c)$	111.4	109.2	110.9	108.8	112.6	110.3	113.4	111.0
$\theta(O_bO_cH)$	98.6	99.2	98.6	98.7	99.5	98.3	94.3	94.1
$\tau(O_aO_bO_cH)$	0.0	180.0	0.0	180.0	0.0	180.0	0.0	180.0
energy	−225.181638^c	−225.179183^c	−225.745970^d	−225.744254^d	−226.154086^e	−226.153907^e	−225.189625^f	−225.190307^f
MRMP2 energy	−225.799956	−225.797636	−225.801923	−225.800460	−225.803443	−225.803822	−225.806023	−225.807292

^{a} Bond lengths R in ångström, and bond angles θ and dihedral angles τ in degrees. ^{b} The cc-pVTZ basis set was used. ^{c} MP2(FC) energy. ^{d} QCISD(FC) energy. ^{e} B3LYP energy. ^{f} CASSCF(19,13) energy.

TABLE 2: Absolute 0 K Energies E_0^a (hartree), Relative^b Energies ΔE_0 (kcal/mol), and Ethalpy Change ΔH_{298}^a (kcal/mol) to Reactants at the MRMP2/CAS(19,13) Levels

	MRMP2/cc-pVTZ			MRMP2/TZV(2df,2p)		
	E_0	ΔE_0	ΔH_{298}	E_0	ΔE_0	ΔH_{298}
O + HO$_2$	−225.695558	0.0	0.0	−225.719283	0.0	0.0
trans-HO$_3$	−225.789870	−59.18	−60.04	−225.812806	−58.69	−59.55
cis-HO$_3$	−225.788434	−58.28	−59.22	−225.811028	−57.57	−58.50
O$_2$ + OH	−225.785494	−56.44	−56.15	−225.808110	−55.74	−55.46

^{a} Zero-point corrections(ZPE) and thermal corrections(H) at the B3LYP/6-311G (d,p) level were used: ZPE(HO$_2$) = 0.014122 a.u., ZPE(*trans*-HO$_3$) = 0.017422 a.u., ZPE(*cis*-HO$_3$) = 0.017589 a.u., ZPE(O$_2$) = 0.003739 a.u., ZPE(OH) = 0.008440 a.u., H(O) = 0.002360 a.u., H(HO$_2$) = 0.017925 a.u., H(*trans*-HO$_3$) = 0.022210 a.u., H(*cis*-HO$_3$) = 0.022261 a.u., H(O$_2$) = 0.007046 a.u., H(OH) = 0.011745 a.u. ^{b} Relative to reactants.

HO$_3$ molecule as meta-stable and gives an incorrect PES, especially toward the product side. In contrast, the PES at the MRMP2/CAS(19,13) level reveals a distinct energy minimum for the HO$_3$ molecule. The energy of the *trans*-HO$_3$ molecule is lower than that of the *cis*-HO$_3$ molecule. The central O$_b$−O$_c$ bond length for the HO$_3$ molecule at the MRMP2/CAS(19,13) level is fairly long (1.75 Å), while that at the CAS(7,7) level is underestimated (1.34 Å). The MRMP2/CAS(19,13) calculation yields a reasonable description of the PES, as shown below.

B. HO$_3$ Geometries and Energies. Table 1 shows the geometries and energy of the *cis*- and *trans*-HO$_3$ molecules optimized at the various levels of theory. The CASSCF geometries are optimized at 0.05 Å intervals for the central O$_b$−O$_c$ bond length, and those with the lowest MRMP2 energies are listed (also see Figure 2). The central O−O bond lengths $R(O_b-O_c)$ for the *cis*- and *trans*-HO$_3$ molecule are 1.433 and 1.437 Å at the MP2 level, 1.461 and 1.475 Å at the QCISD level, 1.503 and 1.544 Å at the B3LYP level, and 1.75 and 1.75 Å at the CASSCF level. $R(O_b-O_c)$ increases in the order of the MP2, QCISD, B3LYP, and CASSCF levels. The difference in $R(O_b-O_c)$ between the *cis*- and *trans*-HO$_3$ molecules also increases in this order, though we could not find a clear difference at the CASSCF level, since the bond lengths are optimized only at 0.05 Å intervals. The energy differences between the *cis*- and *trans*-HO$_3$ molecules were 2.455 mhartree at the MP2 level, 1.716 mhartree at the QCISD level, 0.179 mhartree at the B3LYP level, and −0.068 mhartree at the CASSCF level. Hence, the relative stability of the *trans*-HO$_3$ molecule increases in this order, and a longer $R(O_b-O_c)$ for equilibrium geometry leads to stability of the *trans*-HO$_3$ molecule rather than the *cis*-HO$_3$ molecule.

Next, we calculated the MRMP2/CAS(19,13) energies using geometries optimized at each level; the results are shown in the last column of Table 1. The MRMP2 energies decreased in the order of the MP2 geometry, QCISD geometry, B3LYP geometry, and CASSCF geometry. The B3LYP and CASSCF geometries exhibited lower MRMP2 energies for *trans*-HO$_3$ molecules than for *cis*-HO$_3$ molecules, while the MP2 and QCISD geometries did not. Hence, the level of theory based

on a single reference wave function seems to underestimate the O$_b$−O$_c$ bond length and is therefore misleading in regard to the relative stability of the isomers. Thus, we believe that the MRMP2/CASSCF calculation with larger active space size reasonably describes the HO$_3$ PES, though it has been suggested that the CASSCF theory with small active space underestimates the O$_b$−O$_c$ bond length.[14] It should be noted that, of all the geometries based on a single reference wave function, the B3LYP geometries are the closest to the CASSCF geometries.

C. Reaction Energies. Table 2 shows the energies for the reactants, HO$_3$, and products at the MRMP2/CAS(19,13) level. Unfortunately, the CAS(19,13) calculation does not give an energy minimum stationary point for the HO$_3$ molecule, as shown in Figure 2. Hence, we used the zero-point energies and thermal corrections at the B3LYP/6-311(d,p) level instead of those at the CASSCF level for all stationary points in the MRMP2 calculations in Table 2. The calculated heat at 298 K for the reaction O + HO$_2$ → OH + O$_2$ was compared with the experimental one, 53.7 kcal/mol,[35] and was found to agree to within 2.5 kcal/mol at the MRMP2/cc-pVTZ level and 1.8 kcal/mol at the MRMP2/TZV(2df,2p) level. The *trans*-HO$_3$ molecule lies at 3.9 kcal/mol below the OH + O$_2$ dissociation limit at the MRMP2/cc-pVTZ level and 4.1 kcal/mol below the OH + O$_2$ dissociation limit at the MRMP2/TZV(2df,2p) level; they were compared with the experimental value 10 ± 5 kcal/mol evaluated by the FTICR-MS technique.[17]

D. Interaction and BSSE Energy in the Entrance Channel. As shown above, the title reaction is barrierless for both the entrance and exit channels. The energy difference between the products and the HO$_3$ molecule is very small compared to that between the reactants and the HO$_3$ molecule. An energy-rich HO$_3$ molecule produced in the attractive region in the entrance channel will dissociate toward the products. Hence, there may be a bottleneck in the attractive region that governs the reaction rate, and the location of a generalized transition state may be determined variationally, to minimize the rate constant at each temperature. We chose an approximate minimum energy path as the reference path for the dynamics calculation. For this purpose, the $R(O_a-O_b)$ distance was varied from 1.9 to 2.8 Å

PE Surface and Rate Constant for an O(^{3}P) + HO$_2$ Reaction

J. Phys. Chem. A, Vol. 104, No. 14, 2000 **3207**

TABLE 3: Geometries and Vibrational Frequencies ν (cm^{-1}) along the Reaction Pathway at the CAS(19,13) Level

	CAS(19,13)/cc−pVTZ			CAS(19,13)/TZV(2df,2p)	
s^a	geometries^b	frequencies^c	s^a	geometries^b	frequencies^c
0.000	2.80, 1.351, 0.975, 106.9, 103.2, −76.5	36, 84, 1055, 1435, 3626	0.000	2.80, 1.351, 0.975, 109.4, 103.2, −82.5	32, 113, 1055, 1435, 3630
0.177	2.70, 1.351, 0.975, 109.5, 103.2, −83.4	55, 145, 1053, 1436, 3626	0.223	2.70, 1.351, 0.975, 110.6, 103.2, −83.8	59, 134, 1053, 1435, 3630
0.412	2.60, 1.351, 0.975, 110.2, 103.2, −86.1	79, 192, 1052, 1437, 3629	0.448	2.60, 1.351, 0.975, 110.9, 103.2, −86.2	81, 196, 1054, 1436, 3631
0.652	2.50, 1.352, 0.975, 110.7, 103.2, −87.0	104, 244, 1052, 1437, 3624	0.727	2.50, 1.352, 0.975, 110.8, 103.2, −87.0	102, 237, 1053, 1438, 3634
0.914	2.40, 1.352, 0.975, 110.5, 103.2, −87.0	128, 286, 1046, 1437, 3625	0.979	2.40, 1.352, 0.975, 110.9, 103.2, −87.4	126, 281, 1049, 1438, 3634
1.177	2.30, 1.353, 0.975, 110.1, 103.2, −87.5	153, 337, 1043, 1439, 3627	1.246	2.30, 1.353, 0.975, 110.4, 103.2, −87.7	155, 336, 1042, 1439, 3633
1.442	2.20, 1.354, 0.975, 109.7, 103.1, −87.8	170, 385, 1017, 1438, 3629	1.514	2.20, 1.354, 0.975, 109.8, 103.1, −87.9	168, 392, 1025, 1440, 3621
1.710	2.10, 1.357, 0.975, 109.1, 103.0, −87.7	205, 440, 1012, 1439, 3635	1.781	2.10, 1.357, 0.974, 109.2, 103.1, −87.8	205, 441, 1013, 1440, 3638
2.007	2.00, 1.361, 0.975, 108.5, 102.9, −87.6	251, 486, 993, 1441, 3639	2.048	2.00, 1.361, 0.974, 108.6, 102.9, −87.6	250, 484, 994, 1441, 3644
2.236	1.90, 1.369, 0.974, 107.9, 102.7, −87.2	302, 507, 967, 1441, 3650	2.310	1.90, 1.369, 0.974, 107.9, 102.7, −87.2	301, 509, 968, 1440, 3654

^{a} Mass-scaled coordinate (Bohr). ^{b} The order of $R(O_a-O_b)$, $R(O_b-O_c)$, $R(O_c-H)$, $\theta(O_aO_bO_c)$, $\theta(O_bO_cH)$, and $\tau(O_aO_bO_cH)$; R in ångström, and θ and τ in degrees. ^{c} The order of $O_a-O_b-O_c$ bend, torsion + O_b-O_c-H out-of-plane bend, O_b-O_c stretch, O_b-O_c-H in-plane bend, and O_c-H stretch.

TABLE 4: Relative MRMP2 Energies and BSSE-Corrected Energies (kcal/mol) for Geometries Optimized at the CAS(19,13) Level

	cc-pVTZ	TZV(2df,2p)	TZV(2df,2p)++	
R^a	E^b	E^b	E^b	$E_{corr}{}^c$
2.80	−2.30	−2.26	−2.21	−1.96
2.70	−2.52	−2.48	−2.42	−2.14
2.60	−2.83	−2.73	−2.70	−2.37
2.50	−3.21	−3.14	−3.09	−2.71
2.40	−3.76	−3.68	−3.69	−3.26
2.30	−4.50	−4.47	−4.49	−3.99
2.20	−5.56	−5.59	−5.61	−5.03
2.10	−7.10	−7.17	−7.19	−6.51
2.00	−9.29	−9.40	−9.41	−8.59
1.90	−12.38	−12.47	−12.49	−11.51

^{a} Bond length $R(O_a-O_b)$ in ångström. ^{b} MRMP2 energies relative to the O + HO$_2$ reactant: −225.709680 a.u. for the cc-pVTZ, −225.7334047 a.u. for the TZV(2df,2p), and −225.735482 a.u. for the TZV(2df,2p)++ basis set. ^{c} BSSE-corrected MRMP2 energies relative to the O + HO$_2$ reactant.

with an interval of 0.1 Å, and the other geometric parameters were optimized for each value of $R(O_a-O_b)$ at the CAS(19,-13)/cc-pVTZ or CAS(19,13)/TZV(2df,2p) level. Here, a partial optimization at a distance exceeding 2.8 Å led to a reaction pathway corresponding to the direct hydrogen abstraction reaction by the oxygen atom. These 10 optimized geometries and the harmonic vibrational frequencies, projected out of the gradient direction,[36] are shown in Table 3, and the interaction energies along the O−O$_2$H separation are shown in Table 4.

The MRMP2 calculations may give exaggerated values for the interaction energies of the O−O$_2$H interacting system due to basis set superposition errors (BSSE) caused by the finite basis approximation used in the calculations. We therefore estimated the correction energies using the traditional two-body counterpoise method.[29] Figure 3 shows the BSSE energy components $E_O{}^C$ and $E_{HO_2}{}^C$ at the MRMP2 level along the reaction pathway for the three basis sets used. Both components for the TZV(2df,2p) basis set are smaller than those for the cc-pVTZ basis set. The addition of diffuse functions to the TZV-(2df,2p) basis set decreases the BSSE energies because of the larger basis set space available for interacting electrons. The BSSE-corrected interaction energies at the MRMP2/TZV(2df,-2p)++ level are shown in the last column in Table 4. In this study, the BSSE-corrected PES with the TZV(2df,2p)++ basis set is considered to give a lower bound for the interaction energy and is used to get a lower bound for the kinetic rate constant within the framework of the calculation method used, since the BSSE energy corrected by the counterpoise method generally tends to be overestimated, especially at the correlated level.
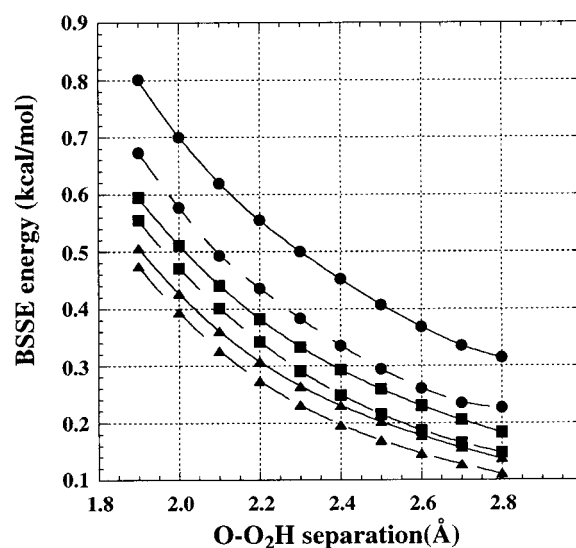
Figure 3. Change in BSSE energy components along reaction pathway: $E_O{}^C$ (solid lines), $E_{HO_2}{}^C$ (dashed lines), cc-pVTZ (circles), TZV(2df,2p) (squares), TZV(2df,2p)++ (triangles).

E. Rate Constant of the Reaction via HO$_3$. The distances between the oxygen atom and the HO$_2$ mass center were calculated for the geometries shown in Table 3 and were converted into the mass-scaled coordinate χ to get the reaction coordinate s for the dynamics calculation. The mass-scaled coordinate is represented as $\chi_{ir} = (m_i/\mu)^{1/2}(R_{ir} - R_{c.m.r})$, $i =$ 1,2, $r = x, y, z$,[30] where $R_{c.m.r}$ is the mass center coordinate and μ is the reduced mass of the reactant-relative translational motion (10.77 amu). The reaction coordinate s in Table 3 is the separation between the O atom and HO$_2$ molecule, represented by the mass-scaled coordinate. The quantities needed for the dynamics calculation of the values of s between those in Table 3 were obtained by the Lagrangian interpolation method, which was implemented in POLYRATE code.
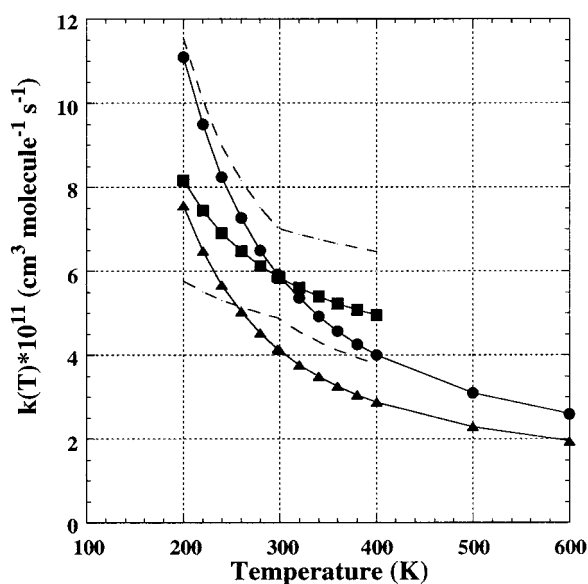
A preliminary rate constant calculation using canonical variational theory, which minimizes a canonical ensemble, indicates that generalized transition states are located within the mass-scaled reaction coordinates considered in Table 3. Thus, for the cc-pVTZ basis set, the s values (in bohr units) for the bottleneck are 0.289 at 200 K, 0.488 at 300 K, and 0.642 at 400 K. They are 0.443 at 200 K, 0.510 at 300 K, and 0.590 at 400 K for the TZV(2df,2p) basis set.

Table 5 shows the μVT rate constants $k_{\mu VT}$ at each temperature; the rate constants $k'_{\mu VT}$ obtained by using the BSSE-corrected PES are also shown in parentheses. The values of $k_{\mu VT}$ are almost equal for all basis sets. Figure 4 shows the temperature dependence of the μVT rate constants obtained by

TABLE 5: μVT Rate Constant $k_{\mu VT}{}^a$ for O–O$_2$H Reaction Channel and TST Rate Constant $k_{TST}{}^b$ for O–HO$_2$ Reaction Channel
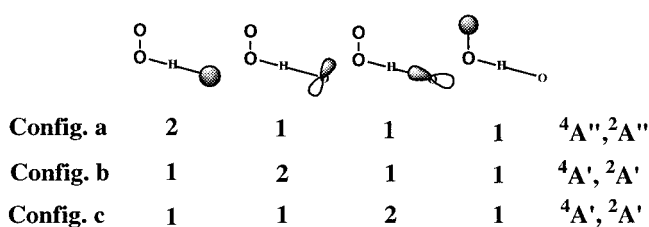
T (K)	O–O$_2$H Reaction $k_{\mu VT}$			O–HO$_2$ Reaction k_{TST}		$k_{exp}{}^f$
	cc-pVTZ	TZV	TZV++	^{4}A	^{2}A	
200	12.0	11.6	11.1 (7.56)^c	1.17 (0.1, 0.0)^d	0.00 (0.0, 0.0)^e	8.2
220	10.2	9.85	9.49 (6.48)	1.10 (0.1, 0.0)	0.00 (0.0, 0.0)	7.4
240	8.79	8.54	8.24 (5.67)	1.04 (0.1, 0.1)	0.01 (0.0, 0.0)	6.9
260	7.73	7.52	7.27 (5.03)	1.00 (0.1, 0.1)	0.01 (0.0, 0.0)	6.5
280	6.88	6.71	6.49 (4.52)	1.00 (0.1, 0.1)	0.01 (0.0, 0.0)	6.1
298	6.26	6.11	5.93 (4.15)	0.98 (0.1, 0.1)	0.02 (0.0, 0.0)	5.9
300	6.20	6.05	5.87 (4.11)	0.97 (0.1, 0.1)	0.02 (0.0, 0.0)	5.8
320	5.64	5.51	5.36 (3.77)	0.95 (0.1, 0.1)	0.02 (0.0, 0.0)	5.6
340	5.18	5.06	4.93 (3.49)	0.96 (0.2, 0.1)	0.02 (0.0, 0.0)	5.4
360	4.79	4.68	4.57 (3.25)	0.94 (0.2, 0.1)	0.03 (0.0, 0.0)	5.2
380	4.45	4.36	4.26 (3.05)	0.96 (0.2, 0.1)	0.03 (0.0, 0.0)	5.1
400	4.17	4.08	4.00 (2.87)	0.97 (0.2, 0.2)	0.04 (0.0, 0.0)	4.9
500	3.20	3.14	3.10 (2.28)	1.06 (0.3, 0.2)	0.06 (0.0, 0.0)	
600	2.66	2.61	2.59 (1.94)	1.20 (0.4, 0.3)	0.09 (0.0, 0.0)	
800	2.10	2.06	2.06 (1.61)	1.62 (0.6, 0.6)	0.18 (0.0, 0.0)	
1000	1.84	1.81	1.82 (1.46)	2.22 (0.9, 0.9)	0.38 (0.1, 0.1)	
1500	1.61	1.60	1.61 (1.35)	4.32 (2.0, 1.9)	0.73 (0.3, 0.2)	

^{a} Units in 10^{-11} cm^3 molecule^{-1} s^{-1}. ^{b} Units in 10^{-11} cm^3 molecule^{-1} s^{-1}. Rate constants with tunneling correction. ^{c} BSSE-corrected potential was used. ^{d,e} Values in parentheses represent the contributions without tunneling correction from the TS1 and TS2 in the ^{4}A state, or the TS3 and TS4 in the ^{2}A state. ^{f} Reference 9. $k = 3.0 \times 10^{-11}$ exp(200/T); 200 K to 400 K.

Figure 4. Temperature dependence for μVT rate constants at the MRMP2/TZV(2df,2p)++ level: experimental upper and lower limit (dashed lines), experimental recommended values (squares), BSSE-uncorrected potential (circles), BSSE-corrected potential (triangles).

Config. a	2	1	1	1	^{4}A'', ^{2}A''
Config. b	1	2	1	1	^{4}A', ^{2}A'
Config. c	1	1	2	1	^{4}A', ^{2}A'

Figure 5. Dominant electron configurations (electron occupancy) of six electronic states involved in hydrogen atom abstraction reaction.

F. PES and Rate Constant of Hydrogen Atom Abstraction Reaction. The PES for the hydrogen atom abstraction reaction was investigated to estimate the contribution of the reaction channel to the overall O + HO$_2$ reaction rate constant. The reaction will have a distinct transition state, as shown by the CASSCF(7,7) calculation,[12] and may contribute to the rate constant at a high temperature. Dupuis et al. have investigated six electronic states involved in the reaction, and have shown that four electronic states, the ^{4}A', ^{4}A'', ^{2}A', and ^{2}A'' states, are responsible for the PESs connecting the reactants and products of the reaction, whereas the remaining a ^{4}A' state and a ^{2}A' state are repulsive toward the products. The dominant electron configurations for the states (*a*, *b*, and *c*) are shown in Figure 5. We optimized the transition state geometry at the CAS(19,-13)/cc-pVTZ level under C$_1$ symmetry and calculated the intrinsic reaction coordinate (IRC) at the 0.01 or 0.02 amu$^{1/2}$ bohr intervals. Figure 6a shows the CASSCF PES along the IRC for the ^{4}A state, where the transition state has a dominant configuration *a*. When the reaction path is followed in the direction of the reactants ($s = -\infty$), the dominant electron configuration in the ground state changes from *a* to *c* near $s = -0.05$ amu$^{1/2}$ bohr. Therefore, we performed the MC-QDPT2 single-point calculations for three nearly degenerate ^{4}A electronic states along the IRC. Here, the MC-QDPT2 calculations were carried out using a state-averaged CASSCF wave function with weights of 1.0, 1.0, and 1.0 for the triple-reference-states. Figure 6b shows the MC-DPT2 PESs for the three ^{4}A electronic states. The two states with configurations *b* and *c* interact with each other. An avoided crossing thus occurs at the *s* value around −0.2 amu$^{1/2}$ bohr because both states are A' states under the C$_s$ symmetry. However, we assume them to be two diabatic states in the kinetic calculation since the interaction is very weak with an energy separation of 0.6 kcal/mol. The two QCPT2

the PES with the TZV(2df,2p)++ basis sets. The temperature dependence of the recommended rate constant is also shown with the upper and lower limit based on uncertainty estimates.[9] The values of $k_{\mu VT}$ are within the experimental upper and lower limits, and are in good agreement with the experimental rate constants, especially those near room temperature. However, the calculated constant exhibits a slightly larger negative temperature dependence than the recommended one. The values of $k'_{\mu VT}$ may provide an estimate for the lower limit of the rate constant at the level of theory in this study. The $k'_{\mu VT}$ was only 15% lower than that of the experimental lower limit (4.8 × 10^{-11} cm^3 molecule^{-1} s^{-1}) at 300 K.

The dynamics calculations were performed with the harmonic vibrational frequencies obtained by the CASSCF calculation. The rate constant increases when the harmonic vibrational frequencies are scaled by a factor less than 1. Though the scale factor at the CASSCF level is not actually known, if we choose 0.95, the rate constant increases by only about 10% at 300 K.

PE Surface and Rate Constant for an O(^{3}P) + HO$_2$ Reaction

J. Phys. Chem. A, Vol. 104, No. 14, 2000 **3209**

TABLE 6: Geometries and Energies of Transition State[a] for Hydrogen Abstraction Reaction Channel

	^{4}A			^{2}A		
	CASSCF	QDPT2(TS1)	QDPT2(TS2)	CASSCF	QDPT2(TS3)	QDPT2(TS4)
$R(O_b-O_c)$	1.2931	1.3134	1.3134	1.2931	1.3106	1.3106
$R(O_c-H)$	1.0927	0.9600	0.9600	1.1056	0.9625	0.9625
$R(H-O_a)$	1.3959	1.5391	1.5391	1.3518	1.5046	1.5046
$\theta(O_bO_cH)$	108.25	105.77	105.77	108.37	106.13	106.13
$\theta(O_c-H-O_a)$	178.83	177.68	177.68	177.79	174.92	74.92
$\tau(O_bO_cHO_a)$	23.19	166.71	166.71	172.08	176.50	176.50
energies	−225.100967	−225.706722	−225.706506	−225.094346	−225.703916	−225.703267
	(15.92)	(3.66)	(3.80)	(20.08)	(5.42)	(5.83)
frequencies[b]		4367i, 153, 350, 509, 1268, 1407			5814i, 183, 491, 554, 1237, 1275	

[a] Bond lengths in Å, angles in deg, energy in a.u. The cc-pVTZ basis sets were used. Structural parameters correspond to $O_b-O_c-H-O_a$. Reactants energies: CASSCF = −225.126340 a.u., QDPT2 = −225.712560 a.u. [b] At the CAS(19,13) level.
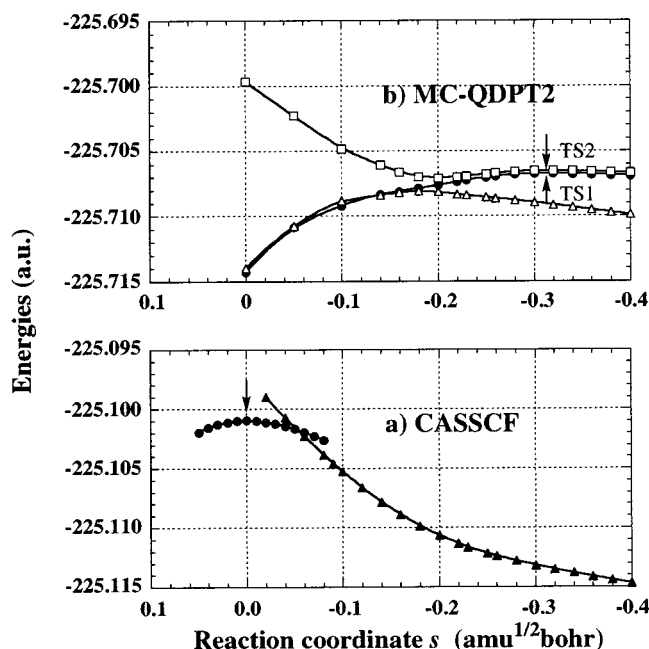

Figure 6. ^{4}A potential energy surface for the hydrogen abstraction reaction at the MC-QDPT2/CAS(19,13)/cc-pVTZ level: filled circles (config. a), filled triangles (config. c), open squares and triangles (config. b + c). Arrows represent the transition states.

transition states are both located at $s = -0.31$ amu$^{1/2}$ bohr toward the reactants from the CASSCF one. We also performed a similar calculation for the ^{2}A PES and found a CASSCF transition state and two MC-QDPT2 transition states. Table 6 summarizes the transition state geometries in the ^{4}A and ^{2}A states, where the ^{4}A and ^{2}A CASSCF transition states have dominant electronic configurations a and b, respectively. The barrier heights decrease more than 10 kcal/mol in both the ^{4}A and ^{2}A states when the dynamic electron correlation is taken into account. The QCPT2 classical barrier height in the ^{4}A state is 3.7 to 3.8 kcal/mol. This is very close to the value 3.5 kcal/mol[12] estimated by Dupuis et al. on the basis of their MC and CI calculations, but is significantly lower than the barrier height of the DMBE PES (18 kcal/mol).[23] The ^{4}A barrier height is 2.0 kcal/mol lower than the ^{2}A barrier height, and thus the reaction in the ^{4}A electronic state is preferred over that in the ^{2}A electronic state.

We calculated the kinetic rate constants based on the conventional transition state theory (TST) using the CASSCF frequencies (excluding imaginary frequencies). The calculated rate constants without tunneling correction are shown in parentheses in Table 5. Since the PES around the QDPT2 transition state is flatter than that around the CASSCF transition state, we must estimate an imaginary frequency along the

reaction coordinate for the QDPT2 PES. A simple estimation with a harmonic approximation gives us 1500i for $\nu_{MC-QDPT2}^{TS1,TS2}$ of the ^{4}A state, and 2000i for $\nu_{MC-QDPT2}^{TS3,TS4}$ of the ^{2}A state. The values of k_{TST} with Wigner tunneling correction using the imaginary frequencies are shown in Table 5. The values of k_{TST} at 200, 300, and 400 K are 10%, 15%, and 25% of the $k_{\mu VT}$ values, respectively. However, it should be noted that the Wigner correction is justifiable only at very high temperature where the value is near unity.[37] We thus believe that the O−O$_2$H reaction channel is preferred over the O−HO$_2$ reaction channel at low temperature, in accordance with the experimental observation.[10] However, the O−HO$_2$ reaction channel contributes significantly to the overall rate constant at high temperatures, and the reaction channel is preferred over the O−O$_2$H reaction channel, especially above 1000 K. The calculated overall rate constant $k_{\mu VT} + k_{TST}$ at high temperature may be compared with the experimental estimate of $k = 5.5 \times 10^{-11}$ cm^3 molecule^{-1} s^{-1} at 1050 K[38] and 8.3 $\times$ 10^{-11} cm^3 molecule^{-1} s^{-1} at 1600 K.[39] The importance of the channel has not been addressed in the previous studies[23,24] because the studies predicted a significantly high barrier for the hydrogen abstraction channel.

Conclusions

We derived the following conclusions. (1) All lone pairs of electrons on the oxygen atoms must be included in the active space in the description of the MRMP2 PES, especially around the HO$_3$ critical structure and in the exit channel. Of all the levels of theory based on a single-reference wave function, the HO$_3$ geometry at the B3LYP level is closest to that at the MRMP2 level. *trans*-HO$_3$ is more stable than *cis*-HO$_3$. The UHF wave function is significantly spin-contaminated even around the HO$_3$ equilibrium structure and will be subject to a more severe spin contamination for a large separation of $R(O-O_2H)$. Thus, we believe that the MRMP2 level of theory gives a precise PES for the open shell system, which cannot be described precisely by the level of theory based on a UHF wave function. The PES in this study is based on the MRMP2 single-point energy with optimization at the CASSCF level. However, a more accurate PES may be obtained by using the MRMP2 energy gradient method.[40] (2) The rate constant based on microcanonical variational theory, which is equivalent to the adiabatic theory of reactions,[41] reproduces the experimental recommended values well within a temperature range of 200−400 K, though the calculated rate constant exhibits a slightly larger negative temperature dependence than the recommended one. This study, therefore, does not support the use of the rate constant decreased by 50% as proposed by Summers et al.[2] in order to resolve the ozone deficit problem. (3) The study of the QCT[23] and quantum mechanical adiabatic approach[24] based on DMBE PES has

3210 *J. Phys. Chem. A, Vol. 104, No. 14, 2000*

Setokuchi et al.

showed little temperature dependence of the rate constant in the range of 200−1600 K. The authors of the study concluded that the bottleneck of the reaction is dominated by a long-range force. The bottlenecks based on canonical variational theory are located at 2.6 Å, which means that a short-range force is also important. (4) The O−HO$_2$ hydrogen atom abstraction reaction is preferred over the O−O$_2$H reaction via HO$_3$ at high temperature, especially above 1000 K.

To determine the atmospheric degradation reaction mechanisms, it is important to evaluate the stability of trioxy radicals such as HO$_3$ precisely. For example, Jungkamp et al.[13] suggested the possibility that the CH$_3$O + O$_2$ reaction proceeds via a CH$_3$O$_3$ intermediate. The possibility of a CH$_3$O$_3$ radical as an intermediate of the CH$_3$O$_2$ + CH$_3$O$_2$ reaction is now being investigated in our laboratory.

References and Notes

(1) Jucks, K. W.; Johnson, D. G.; Chance, K. V.; Traub, W. A.; Margitan, J. J.; Osterman, G. B.; Salawitch, J. R.; Sasano, Y. *Geophys. Res. Lett.* **1998**, *25*, 3935.

(2) Summers, M. E.; Conway, R. R.; Siskind, D. E.; Stevens, M. H.; Offermann, D.; Riese, M.; Preusse, P.; Strobel, D. F.; Russell, J. M., III. *Science* **1997**, *277*, 1967.

(3) Crutzen, P. *Science* **1997**, *277*, 1951.

(4) Keyser, L. F. *J. Phys. Chem.* **1982**, *86*, 3439.

(5) Sridharan, U. C.; Qiu, L. X.; Kaufman, F. *J. Phys. Chem.* **1982**, *86*, 4569.

(6) Ravishankara, A. R.; Wine, P. H.; Nicovich, J. M. *J. Chem. Phys.* **1983**, *78*, 6629.

(7) Brune, W. H.; Schwab, J. J.; Anderson, J. G. *J. Phys. Chem.* **1983**, *87*, 4503.

(8) Nicovich, J. M.; Wine, P. H. *J. Phys. Chem.* **1987**, *91*, 5118.

(9) DeMore, W. B.; Sander, S. P.; Golden, D. M.; Hampson, P. F.; Kurylo, M. J.; Howard, C. J.; Ravishankara, A. R.; Kolb, C. E.; Molina, M. J. *Chemical Kinetics and Photochemical Data for Use in Stratospheric Modeling*; Evaluation No. 12; NASA, Jet Propulsion Laboratory: Pasadena, CA, 1997; Publ. 97-4.

(10) Sridharan, U. C.; Klein, F. S.; Kaufman, F. *J. Phys. Chem.* **1985**, *82*, 592.

(11) Mathisen, K. B.; Siegbahn, P. E. M. *Chem. Phys.* **1984**, *90*, 225.

(12) Dupuis, M.; Fitzgerald, G.; Hammond, B.; Lester, W. A., Jr.; Schaefer, H. F., III. *J. Chem. Phys.* **1986**, *84*, 2691.

(13) Jungkamp, T. P. W.; Seinfeld, J. H. *Chem. Phys. Lett.* **1996**, *257*, 15.

(14) Vincent, M. A.; Hillier, I. H. *J. Phys. Chem.* **1995**, *99*, 3109.

(15) Vincent, M. A.; Hillier, I. H.; Burton, N. A. *Chem. Phys. Lett.* **1995**, *233*, 111.

(16) Vincent, M. A.; Burton, N. A.; Hillier, I. H. *Mol. Phys.* **1996**, *87*, 945.

(17) Speranza, M. *Inorg. Chem.* **1996**, *35*, 6140.

(18) Speranza, M. *J. Phys. Chem. A* **1998**, *102*, 7535.

(19) Hirao, K. *Chem. Phys. Lett.* **1992**, *190*, 374; **1992**, *196*, 397; **1993**, *201*, 59.

(20) Hirao, K. *Int. J. Quantum Chem.* **1992**, *S26*, 517.

(21) Nakano, H. *J. Chem. Phys.* **1993**, *99*, 7983.

(22) Nakano, H. *Chem. Phys. Lett.* **1993**, *207*, 372.

(23) Wang, W.; González-Jonte, R.; Varandas, A. J. C. *J. Phys. Chem. A* **1998**, *102*, 6935.

(24) Varandas, A. J. C.; Szichman, H. *Chem. Phys. Lett.* **1998**, *295*, 113.

(25) Varandas, A. J. C.; Yu, H. G. *Mol. Phys.* **1997**, *91*, 301.

(26) Dunning, T. H. *J. Chem. Phys.* **1989**, *90*, 1007.

(27) Huzinaga, S. *J. Chem. Phys.* **1965**, *42*, 1293.

(28) Dunning, T. H. *J. Chem. Phys.* **1971**, *55*, 716.

(29) Boys, S. F.; Bernardi, F. *Mol. Phys.* **1970**, *19*, 553.

(30) Truhlar, D. G.; Isaacson, A. D.; Garrett, B. C. *The Theory of Chemical Reaction Dynamics*; Baer, M., Ed.; CRC Press: Boca Raton, FL, 1985; *4*, 65.

(31) Rai, S. N.; Truhlar, D. G. *J. Chem. Phys.* **1983**, *79*, 6046.

(32) Schmidt, M. W.; Baldridge, K. K.; Boatz, J. A.; Elbert, S. T.; Gorden, M. S.; Jensen, J. H.; Koseki, S.; Matsunaga, M.; Nguyen, K. A.; Su, S.; Windus, T. L.; Dupuis, M.; Montgomery, J. A. *J. Comput. Chem.* **1993**, *14*, 1347.

(33) Frisch, M. J.; Trucks, G. W.; Schlegel, H. B.; Gill, P. M. W.; Johnson, B. G.; Robb, M. A.; Cheeseman, J. R.; Keith, T.; Petersson, G. A.; Montgomery, J. A.; Raghavachari, K.; Al-Laham, M. A.; Zakrzewski, V. G.; Ortiz, J. V.; Foresman, J. B.; Cioslowski, J.; Stefanov, B. B.; Nanayakkara, A.; Challacombe, M.; Peng, C. Y.; Ayala, P. Y.; Chen, W.; Wong, M. W.; Andres, J. L.; Replogle, E. S.; Gomperts, R.; Martin, R. L.; Fox, D. J.; Binkley, J. S.; Defrees, D. J.; Baker, J.; Stewart, J. P.; Head-Gordon, M.; Gonzalez, C.; Pople, J. A. *Gaussian 94*, Gaussian, Inc.: Pittsburgh, PA, 1995.

(34) Corchado, J. C.; Chuang, Y.-Y.; Fast, P. L.; Villà, J.; Coitiño, E. L.; Hu, W.-P.; Liu, Y.-P.; Lynch, G. C.; Nguyen, K. A.; Jackels, C. F.; Gu, M. Z.; Rossi, I.; Clayton, S.; Melissas, V. S.; Steckler, R.; Garrett, B. C.; Isaacson, A. D.; Truhlar, D. G. *POLYRATE*; version 7.9.1; University of Minnesota: Minneapolis, 1998.

(35) Atkinson, R.; Baulch, D. L.; Cox, R. A.; Hampson, R. F., Jr.; Kerr, J. A.; Rossi, M. J.; Troe, J. *J. Phys. Chem. Ref. Data* **1997**, *26*, 521.

(36) Miller, W. H.; Handy, N. C.; Adams, J. E. *J. Chem. Phys.* **1980**, *72*, 99.

(37) Baldridge, K. K.; Gordon, M. S.; Steckler, R.; Truhlar, D. G. *J. Phys. Chem.* **1989**, *93*, 5107.

(38) Day, M. J.; Thompson, K.; Dixon-Lewis G. *Symp. (Int.) Combust., [Proc.]* **1973**, *14*, 47.

(39) Peeters, J.; Mahnen, G. *Symp. (Int.) Combust., [Proc.]* **1973**, *14*, 133.

(40) Nakano, H.; Hirao, K.; Gordon, M. S. *J. Chem. Phys.* **1998**, *108*, 5660.

(41) Garrett, B. C.; Truhlar, D. G. *J. Chem. Phys.* **1979**, *83*, 1052.